Construction of Symmetric Tight Wavelet Frames from Quasi-Iinterpolatory Subdivision Masks and Their Applications

by

Byeongseon Jeong, Myungjin Choi, and Hong Oh Kim

Applied Mathematics
Research Report
07-01
January 19, 2007

DEPARTMENT OF MATHEMATICAL SCIENCES

KAIST 한국과학기술원
Korea Advanced Institute of Science and Technology

International Journal of Wavelets, Multiresolution and Information Processing

CONSTRUCTION OF SYMMETRIC TIGHT WAVELET FRAMES FROM QUASI-INTERPOLATORY SUBDIVISION MASKS AND THEIR APPLICATIONS *

BYEONGSEON JEONG†

Department of Mathematical Sciences, Korea Advanced Institute of Science and Technology, 373-1 Guseong-dong Yuseong-gu, Daejeon, Republic of Korea
kxantera@kaist.ac.kr

MYUNGJIN CHOI

Department of Mathematical Sciences, Korea Advanced Institute of Science and Technology, 373-1 Guseong-dong Yuseong-gu, Daejeon, Republic of Korea,
prime@satrec.kaist.ac.kr

HONG OH KIM

Department of Mathematical Sciences, Korea Advanced Institute of Science and Technology, 373-1 Guseong-dong Yuseong-gu, Daejeon, Republic of Korea
hkim2715@hotmail.com

Received (Day Month Year)
Revised (Day Month Year)
Communicated by (xxxxxxxxxx)

This paper presents tight wavelet frames with two compactly supported symmetric generators of more than one vanishing moments in Unitary Extension Principle. We determine all possible free tension parameters of the quasi-interpolatory subdivision masks whose corresponding refinable functions guarantee our wavelet frame. In order to reduce shift variance of the standard discrete wavelet transform, we use the three times oversampling filter bank and eventually obtain a ternary (low, middle, high) frequency scale. In applications to signal/image denoising and erasure recovery, the results demonstrate reduced shift variance and better performance of our wavelet frame than the usual wavelet systems such as Daubechies wavelets.

Keywords: Wavelet; framelet; quasi-interpolatory subdivision; denoising.

AMS Subject Classification: 22E46, 53C35, 57S20

1. Introduction

Since the construction of the orthonomal or biorthogonal wavelet bases in $L^2(\mathbb{R})$ was introduced in the late 1980s, the construction of the wavelet bases has been

*This work was supported by Korea Research Foundation under Grant KRF-2006-311-D00190.
†Corresponding author

a major subject in many areas such as functional analysis, approximation theory, variational method, signal/image processing, and so forth. Recently, a redundant or overcomplete system, called frame, has emerged as an extension of the wavelet basis because of its flexibility for applications. For practical purposes, recent studies have focused on finding the fewest number of smooth frame generators with symmetry and compact support whose affine transforms generate a tight wavelet frame. Tight wavelet frames with these properties were obtained based on a multiresolution analysis (MRA) by several studies. The standard tight wavelet frames can be constructed by use of the Unitary Extension Principle (UEP),[14] or more extended versions.[5 8] In Ref. 4, the authors provided a criterion for the existence of two compactly supported generators and also a constructive proof of the existence of three symmetric compactly supported generators whose wavelets form tight frames. We attempt to construct tight wavelet frames with two symmetric generators of compact support.

The approximation order of an MRA given by the refinable function is important for effective approximation to functions with the wavelet system. Two types of refinable functions of high approximation order with short support, B-splines and interpolatory refinable functions are used to construct wavelet systems with high approximation orders. However, these refinable functions have drawbacks with respect to constructing tight wavelet frames. In the case of B-splines, for the UEP tight wavelet frames, at least one of the generators has one vanishing moment.[4] The vanishing moments are important for effective representation or the compression of functions in the sense that a wavelet system with higher vanishing moments is more likely to generate wavelet coefficients with higher sparsity. In the case of interpolatory refinable functions with compact support, it is not possible for other refinable functions except for a piecewise linear B-spline to construct a tight wavelet frame with two symmetric generators. See Ref. 13. In some works these drawbacks are overcome by relaxing certain conditions. In Ref. 5, to maximize the vanishing moments of the wavelet frame generators, the authors use the vanishing moment recovery function in the Oblique Extension Principle, which is not easy to find in general. In Ref. 1, the authors sacrifice the compact support of the generators for the construction of a tight wavelet frame using the interpolatory refinable functions. As a consequence, the filter lengths are not finite.

In this paper, we sacrifice the length of support of the wavelets slightly to construct tight wavelet frames with two compactly supported symmetric generators. Instead of B-splines or interpolatory refinable functions, we take the quasi-interpolatory refinable functions proposed in Ref. 3. The quasi-interpolatory refinable functions have approximation orders as high as those of the Deslauriers-Dubuc's interpolatory refinable functions,[3] and the derived wavelet frame generators have more than one vanishing moments. In terms of the wavelet filters, we use quasi-interpolatory subdivision masks, suggested in Ref. 3, as low pass filters instead of B-spline or interpolatory filters. The quasi-interpolatory subdivision masks have a free tension parameter to control the shape of the limit functions and the corre-

sponding refinable functions reproduce polynomials up to the degree corresponding to the length of the masks. We have to determine the free tension parameter in each degree to obtain the tight wavelet frames with two symmetric generators. Due to the computational complexity, we only deal with masks of degrees up to five to construct our wavelet systems. For the wavelet bases other than the frame, Kim et al. recently constructed biorthogonal wavelet systems from quasi-interpolatory subdivision masks and found a general formula for masks of even degrees.[11]

An important issue in signal and image processing is the shift invariance of the wavelet transforms. The standard wavelet transform is not shift invariant because of the down and up sampling process, and thus produces annoying artifacts in the signal and image processing results. In this paper, we relieve these artifacts by employing a three times oversampling filter bank, as shown in Figure 2.[15] The three times oversampling filter bank has a band pass channel without down and up sampling, thus reducing the shift variance to certain extent. We do not use a fully shift invariant filter bank because it imposes a large time cost and space consuming redundancy although it presents no artifact. The empirical results of the denoising and the erasure recovery for the three times oversampling filter bank are satisfactory although they contain a few artifacts. To use this filter bank, we need three wavelet frame generators, say ψ_1, ψ_2, and ψ_3. Note that ψ_3 in our construction is the half shift version of ψ_2. Therefore, we have essentially two wavelet frame generators ψ_1 and ψ_2. Additionally, the wavelet systems constructed in this paper have a ternary frequency scale, which means that the frequency responses of the high and low pass filters are symmetric about those of the band pass filters. This may be useful in some applications that demand uniform partitions of the frequency responses of the filters, for example, audio signal processing, economic time series analysis, and so on.

As a result, all the possible values of the tension parameter ω guaranteeing the tight wavelet frame with two symmetric generators are determined and presented in Table 2. It is very interesting that only particular values of the tension parameter allow us two symmetric generators. The smoothnesses and approximation orders of the refinable functions, as well as the vanishing moments of the wavelet frame generators of the corresponding tension parameter ω's, are computed and summarized in Table 5 and 6.

In addition to the construction of tight wavelet frames, some applications to signal/image denoising and erasure recovery are presented. To measure the performance of our wavelet frame in applications, the standard wavelet systems such as Daubechies wavelets are employed. In signal and image denoising, signals and images denoised by our wavelet frame have only a few or no distortions, while the results by Daubechies wavelet systems have annoying distortions. In terms of errors between original and denoised objects, our wavelet frame presents smaller root mean square errors than Daubechies wavelet systems. Predictably, this is because of reduced shift variance and redundancy of our wavelet frame. In erasure recovery, Daubechies wavelet systems do not work since they are not redundant. Only

redundant wavelet frames as ours can recover erasures of images.

Through the paper, we assume the following terminologies for clarity. The dyadic dilations $2^{j/2}f(2^j\cdot), j \in \mathbb{Z}$ and the integer translations $f(\cdot - k), k \in \mathbb{Z}$ of a function f are called affine transforms. We call the family $\{\phi_{j,k} := 2^{j/2}\phi(2^j \cdot -k), \psi_{i,j,k} := 2^{j/2}\psi_i(2^j \cdot -k)\}$ of the affine transforms of the refinable function ϕ and the mother wavelet ψ_i's the wavelet (resp. framelet) system if the affine transforms of the mother wavelets constitute a basis (resp. frame) for $L_2(\mathbb{R})$. In the case of a wavelet frame, the mother wavelets are called mother framelets to distinguish them from mother wavelets whose affine transforms constitute a basis. We also assume that symmetry addresses in both cases of symmetry and antisymmetry.

2. Construction of Symmetric Tight Wavelet Frames

A tight frame $\{f_k : k \in \mathbb{Z}\}$ is an overcomplete system for $L_2(\mathbb{R})$ which permits the representation of functions as

$$f = \sum_{k\in\mathbb{Z}} \langle f, f_k\rangle f_k, \quad \forall f \in L_2(\mathbb{R}) \tag{2.1}$$

where $\langle\cdot\ ,\cdot\rangle$ is the given inner product in $L_2(\mathbb{R})$. If a sufficiently regular function satisfies the refinement equation

$$\phi(x) = \sqrt{2}\sum_{k\in\mathbb{Z}} h_{0,k}\phi(2x-k), \tag{2.2}$$

it is said to be refinable. Given a refinable function, we can construct a tight wavelet frame $\{\psi_{i,j,k} : i = 1, 2, ..., n, j, k \in \mathbb{Z}\}$ where $\psi_{i,j,k} := 2^{j/2}\psi_i(2^j \cdot -k)$ by defining mother framelet ψ_i's as

$$\psi_i(x) := \sqrt{2}\sum_{k\in\mathbb{Z}} h_{i,k}\phi(2x-k), \quad i = 1, 2, ..., n, \tag{2.3}$$

provided that the filters $h_i := (h_{i,k})_{k\in\mathbb{Z}}$ satisfy the UEP condition of Theorem 2.1 below. A function f in $L_2(\mathbb{R})$ of the representation (2.4) can have the multiresolution representations (2.5) and (2.6) as

$$f = \sum_{k\in\mathbb{Z}} \langle f, \phi_{m,k}\rangle\phi_{m,k} \tag{2.4}$$

$$= \sum_{k\in\mathbb{Z}} \langle f, \phi_{m-1,k}\rangle\phi_{m-1,k} + \sum_{i=1}^{n}\sum_{k\in\mathbb{Z}} \langle f, \psi_{i,m-1,k}\rangle\psi_{i,m-1,k} \tag{2.5}$$

...

$$= \sum_{k\in\mathbb{Z}} \langle f, \phi_{0,k}\rangle\phi_{0,k} + \sum_{i=1}^{n}\sum_{j=0}^{m-1}\sum_{k\in\mathbb{Z}} \langle f, \psi_{i,j,k}\rangle\psi_{i,j,k}. \tag{2.6}$$

The relations (2.2) and (2.3) are equivalent to the Fourier transformed versions

$$\hat{\phi}(\xi) = \frac{1}{\sqrt{2}} H_0(\xi/2)\hat{\phi}(\xi/2), \tag{2.7}$$

$$\hat{\psi}_i(\xi) = \frac{1}{\sqrt{2}} H_i(\xi/2)\hat{\phi}(\xi/2),\ i = 1, 2, ..., n, \tag{2.8}$$

where $H_l(\xi) = \sum_{k\in\mathbb{Z}} h_{l,k} e^{-ik\xi},\ l = 0, 1, 2, ..., n$, called symbols of ϕ and ψ_i's. The symbols are also represented with z-transform, i.e., $H_l(z) = \sum_{k\in\mathbb{Z}} h_{l,k} z^k$, substituting $z = e^{-ik\xi}$ in the context. Define the symbol matrix $H(z)$ consisting of the above symbols as

$$H(z) := \begin{pmatrix} H_0(z) & H_1(z) & ... & H_n(z) \\ H_0(-z) & H_1(-z) & ... & H_n(-z) \end{pmatrix}. \tag{2.9}$$

Given the symbol H_0, we are able to construct tight wavelet frames by determining the other symbols H_i's satisfying certain conditions due to the following theorems.

Theorem 2.1. [14] (Unitary Extension Principle) *If*

$$H(z)H(1/z)^T = 2I, \tag{2.10}$$

then the family $\{\psi_{i,j,k} : i = 1, 2, ..., n, j, k \in \mathbb{Z}\}$ *constitutes a tight frame for* $L_2(\mathbb{R})$.

The above theorem provides us with a sufficient condition in order for the family $\{\psi_{i,j,k}\}$ to be a tight frame for $L_2(\mathbb{R})$. The following theorem provides the necessary and sufficient condition for the existence of the solutions to the matrix equation (2.10).

Theorem 2.2. [4] *The equation (2.10) has a solution if and only if*

$$H_0(z)H_0(1/z) + H_0(-z)H_0(-1/z) \leq 2. \tag{2.11}$$

For the practical reason, fewer number of compactly supported mother framelets with symmetry are preferred. The following theorems tell us about the existence and the criterion for symbols with finite degree, i.e., Laurent polynomials of z.

Theorem 2.3. [4] *For a symmetric Laurent polynomial* H_0*, there are three symmetric Laurent polynomial* H_1*,* H_2*,* H_3 *satisfying (2.10).*

Theorem 2.4. [13] *Let* H_0 *be a Laurent polynomial of degree n satisfying (2.11). Then two symmetric Laurent polynomials* H_1 *and* H_2 *satisfying (2.10) exist if and only if all roots of Laurent polynomial*

$$2 - H_0(z)H_0(1/z) - H_1(z)H_1(1/z) \tag{2.12}$$

have even multiplicity. Moreover, in this case polynomials H_1*,* H_2 *of degree at most n can be chosen.*

In this paper, due to the three times oversampling filter bank, we construct compactly supported tight wavelet frames with symmetry from three mother framelets

(but essentially two), meaning that four Laurent polynomial symbols H_0, H_1, H_2, H_3 are required. Note that as already mentioned in the previous section, our tight wavelet frames are constructed from the essentially two generators ψ_1 and ψ_2 corresponding to the symbols H_1 and H_2, respectively since $\psi_3(\cdot) = \psi_2(\cdot - 1/2)$ (or $H_3(z) = zH_2(z)$). The method to determine the symbols is similar to that in the proof of Theorem 2.3 and that of Ref. 15. We take the quasi-interpolatory subdivision masks of Ref. 3 as the coefficients of H_0 and write H_0 as

$$H_0(z) := \frac{1}{\sqrt{2}} \sum_{k=0}^{n} a_k z^k, \tag{2.13}$$

where a_k's are the quasi-interpolatory subdivision masks presented in Table 1. As one can see, the masks are symmetric. Define H_1 using H_0 as

$$H_1(z) := \begin{cases} z^n H_0(-1/z) & \text{if } n \text{ is odd,} \\ z^{n+1} H_0(-1/z) & \text{if } n \text{ is even,} \end{cases} \tag{2.14}$$

where n is the degree of H_0. Also, define H_3 using H_2 as

$$H_3(z) := zH_2(z). \tag{2.15}$$

Then, the matrix equation (2.10) is reduced as

$$H_0(z)H_0(1/z) + H_0(-z)H_0(-1/z) + 2H_2(z)H_2(1/z) = 2. \tag{2.16}$$

Therefore, H_2 is determined by the spectral factorization of

$$A(z) := 2 - H_0(z)H_0(1/z) - H_0(-z)H_0(-1/z) \tag{2.17}$$

provided that the condition (2.11) and the criterion in Theorem 2.4 are satisfied. Due to our construction method and symmetry of the subdivision masks, the frequency spectra of symbols are ternary as Figure 1. In the aspect of the filter bank, our filter

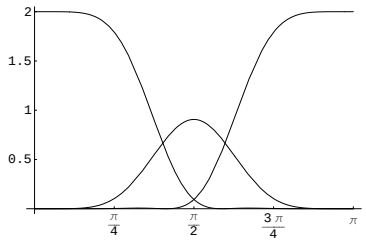

Fig. 1. Frequency spectra $|H_0|^2$(left), $|H_1|^2$(right), and $|H_2|^2$(middle).

system has three times oversampling rate as Figure 2. Since the third channel does not perform the down and up sampling, it reduces the shift variance of the filter system.

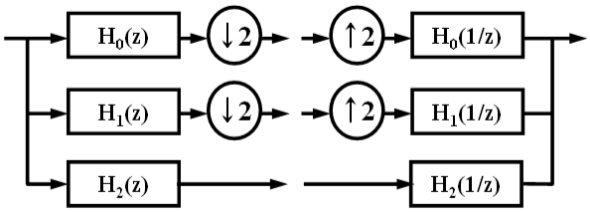

Fig. 2. Filterbank with three times oversampling rate.

3. Results from Quasi-Interpolatory Subdivision Masks

We show the practical computations to obtain the framelet filters. Due to the computational complexity, the computations are restricted to the case of the degree from 1 to 5 of the quasi-interpolatory subdivision masks. Table 1 from Ref. 3 shows the subdivision masks of the degree up to 5.

Table 1. The quasi-interpolatory subdivision masks of the degree from 1 to 5.

Degree	Mask
1	$[\omega, 1-\omega, 1-\omega, \omega]$
2	$[\omega, \frac{1}{2}, 1-2\omega, \frac{1}{2}, \omega]$
3	$[-\omega, -\frac{3}{32}+\omega, \frac{5}{32}+3\omega, \frac{15}{16}-3\omega, \frac{15}{16}-3\omega, \frac{5}{32}+3\omega, -\frac{3}{32}+\omega, -\omega]$
4	$[-\omega, -\frac{1}{16}, 4\omega, \frac{9}{16}, 1-6\omega, \frac{9}{16}, 4\omega, -\frac{1}{16}, -\omega]$
5	$[\omega, \frac{35}{2048}-\omega, -\frac{45}{2048}-5\omega, -\frac{63}{512}+5\omega, \frac{105}{512}+10\omega, \frac{945}{1024}-10\omega, \frac{945}{1024}-10\omega, \frac{105}{512}+10\omega, -\frac{63}{512}+5\omega, -\frac{45}{2048}-5\omega, \frac{35}{2048}-\omega, \omega]$

As one can see, there is a free tension parameter ω in the mask of each degree. Our task is to determine the parameter ω which guarantees the symmetric tight wavelet frame. We present the actual computation by the aid of the mathematical software, MATHEMATICA only for the case of the degree 5. The other cases are similar and can be done even by hand. Firstly, define the symbol H_0 from the masks of the degree 5 as

$$\begin{aligned} H_0(z) = \frac{1}{\sqrt{2}}(\omega + (\frac{35}{2048}-\omega)z + (-\frac{45}{2048}-5\omega)z^2 + (-\frac{63}{512}+5\omega)z^3 \\ + (\frac{105}{512}+10\omega)z^4 + (\frac{945}{1024}-10\omega)z^5 + (\frac{945}{1024}-10\omega)z^6 \\ + (\frac{105}{512}+10\omega)z^7 + (-\frac{63}{512}+5\omega)z^8 + (-\frac{45}{2048}-5\omega)z^9 \\ + (\frac{35}{2048}-\omega)z^{10} + \omega z^{11}). \end{aligned} \tag{3.1}$$

The Laurent polynomial $A(z)$ defined by $H_0(z)$ in the previous section can be

factorized as

$$\begin{aligned} A(z) = \frac{1}{2097152z^{10}}(z-1)^6(z+1)^6((4194304\omega^2 - 71680\omega)z^8 \\ + (-16777216\omega^2 + 352256\omega + 1575)z^6 \\ + (25165824\omega^2 - 2658304\omega - 16590)z^4 \\ + (-16777216\omega^2 + 352256\omega + 1575)z^2 \\ + (4194304\omega^2 - 71680\omega)). \end{aligned} \tag{3.2}$$

Determine the parameter ω which guarantees that $A(z)$ is nonnegative for $z = e^{-i\xi}$ as the following.
Factorize $A(z)$ as

$$\begin{aligned} A(z) &= (2\omega^2 - \frac{35}{1024}\omega)(z^{10} + \frac{1}{z^{10}}) + (-20\omega^2 + \frac{191}{512}\omega + \frac{1575}{2097152})(z^8 + \frac{1}{z^8}) \\ &+ (90\omega^2 - \frac{2855}{1024}\omega - \frac{3255}{262144})(z^6 + \frac{1}{z^6}) + (-240\omega^2 + \frac{1405}{128}\omega + \frac{31185}{524288})(z^4 + \frac{1}{z^4}) \\ &+ (420\omega^2 - \frac{12251}{512}\omega - \frac{36225}{262144})(z^2 + \frac{1}{z^2}) + (-504\omega^2 + \frac{7885}{256}\omega + \frac{189525}{1048576}), \end{aligned} \tag{3.3}$$

change the variable with $z^n + \frac{1}{z^n} = 2\cos n\xi$ as

$$\begin{aligned} &= (4\omega^2 - \frac{35}{512}\omega)\cos 10\xi + (-40\omega^2 + \frac{191}{256}\omega + \frac{1575}{1048576})\cos 8\xi \\ &+ (180\omega^2 - \frac{2855}{512}\omega - \frac{3255}{131072})\cos 6\xi + (-480\omega^2 + \frac{1405}{64}\omega + \frac{31185}{262144})\cos 4\xi \\ &+ (840\omega^2 - \frac{12251}{256}\omega - \frac{36225}{131072})\cos 2\xi + (-504\omega^2 + \frac{7885}{256}\omega + \frac{189525}{1048576}), \end{aligned} \tag{3.4}$$

reform the equation as

$$\begin{aligned} &= -2048(1-\cos^2\xi)^5\omega^2 + (1-\cos^2\xi)^3(35(1-\cos^2\xi)^2 + 8(1-\cos^2\xi) + 64)\omega \\ &+ \frac{105}{8192}(1-\cos^2\xi)^3(15(1-\cos^2\xi) + 32), \end{aligned} \tag{3.5}$$

and change the variable with $y = 1 - \cos^2\xi$ as

$$= ((-2048\omega^2 + 35\omega)y^2 + (8\omega + \frac{1575}{8192})y + (64\omega + \frac{105}{256}))y^3. \tag{3.6}$$

By inspecting the zeros of the last polynomial where $0 \le y \le 1$, we obtain the range of the parameter ω such that $A(z)$ is nonnegative as

$$-\frac{21}{4096} \le \omega \le \frac{235}{4096}. \tag{3.7}$$

Next, we have to determine the parameter ω which admits that all the zeros of $A(z)$ have even multiplicities. As one can see in the equation (3.2), it is enough to verify that all the zeros of the following polynomial have even multiplicities instead of the

whole $A(z)$.

$$\begin{aligned} p(z) := &(4194304\omega^2 - 71680\omega)z^8 + (-16777216\omega^2 + 352256\omega + 1575)z^6 \\ &+ (25165824\omega^2 - 2658304\omega - 16590)z^4 + (-16777216\omega^2 + 352256\omega + 1575)z^2 \\ &+ (4194304\omega^2 - 71680\omega) \end{aligned} \tag{3.8}$$

Since the polynomial $p(z)$ of the degree 8 is even, it is considered as a polynomial of z^2 of the degree 4. In this case, it must be factorized into the multiple of two perfect square forms of quadratic polynomials. By this reasoning, the following lemma can be proved easily for the case of the symmetric polynomial $p(z)$ as ours.

Lemma 3.1. *Let $p(z)$ be the symmetric even polynomial defined by*

$$p(z) = az^8 + bz^6 + cz^4 + bz^2 + a, (a \neq 0). \tag{3.9}$$

Assume that $b \neq 0$. Then, all the zeros of $p(z)$ have even multiplicities if and only if

$$b^2 - 4ac = -8a^2. \tag{3.10}$$

In this case, the zeros are

$$z = \pm\sqrt{-\frac{b}{4a} \pm \sqrt{\left(\frac{b}{4a}\right)^2 - 1}}. \tag{3.11}$$

If $b = 0$, then all the zeros of $p(z)$ have even multiplicities if and only if

$$c = \pm 2a. \tag{3.12}$$

In this case, the zeros are

$$z = \begin{cases} \pm\frac{\sqrt{2}}{2} \pm \frac{\sqrt{2}}{2}i & \text{if } c = 2a, \\ \{\pm 1, \pm i\} & \text{if } c = -2a. \end{cases} \tag{3.13}$$

By Lemma 3.1, we obtain the parameter ω's as

$$\omega = \frac{25(13 \pm 5\sqrt{37})}{65536}, \frac{21}{32768}. \tag{3.14}$$

Finally, we have the parameter ω's as $\frac{25(13+5\sqrt{37})}{65536}$ and $\frac{21}{32768}$ which are contained in the interval (3.7). The symbol H_2 is then obtained by the spectral factorization of $A(z)$. Table 2 shows all the ω's of the degree from 1 to 5 which permits our symmetric tight wavelet frames. As one can see in Table 2, the resulting free tension parameters are of not numerical but algebraic forms except for the case of degree 5. One might obtain algebraic form even for the case of degree 5 after the tedious and complex computation. Also, it is very interesting that only particular values of parameters guarantee our wavelet frame.

Table 3 and 4 presents the filters in the case of the degree from 1 to 5. Note that the filter $h_3 := (h_{3,k})_{k=0}^n$ which is not seen in Table 3 and 4 is just the one shift

Table 2. The tension parameter ω's of the degree from 1 to 5 guaranteeing our symmetric tight wavelet frames.

Degree	ω
1	$[0, 1)$
2	$\frac{1\pm\sqrt{2}}{4}$
3	$-\frac{1}{64}, \frac{15}{64}$
4	n/a
5	$\frac{25(13+5\sqrt{37})}{65536}, \frac{21}{32768}$

version of the filter $h_2 := (h_{2,k})_{k=0}^n$. By this reason, the third channel in the filter bank does not have the down and up sampling process.

Figure 13 presents some of the refinable function ϕ's and the mother framelets ψ_1's and ψ_2's in each degree with the corresponding tension parameter ω's. Note that the mother framelet ψ_3 which is not seen in Figure 13 is the half shift version of ψ_2.

Table 5 shows the smoothness and the vanishing moments of the refinable functions and the framelets with various parameters in the degree L = 1, 2, 3, 4, and 5. Note that the maximum smoothness in each degree is included as a reference. Table 6 shows the approximation orders of the refinable functions and the vanishing moments of our framelets with various parameters in the degree L = 1, 2, 3, and 5.

4. Applications

In this section, the applications of our framelet systems to signal and image processing are provided. To determine the performance of our framelet systems in the applications, Daubechies's orthonomal and biorthogonal wavelet systems are employed. Specifically, we compare the framelet system (F_5) generated by the tension parameter $\omega = \frac{25(13+5\sqrt{37})}{65536}$ in the case of the degree 5 of the subdivision mask with Daubechies's orthonomal wavelet 3 (D_3) and biorthogonal wavelet (7,9) (D(7,9)) systems. D_3 and D(7,9) have the vanishing moments of 3 and 4, respectively, while F_5 has that of 3. In spite that D(7,9) has the different vanishing moment, it is employed due to its popularity in many applications.

4.1. *Signal denoising*

For signal denoising, we use a real data as the original signal extracted from a 2D-image named "Peppers.jpg". The original signal is presented in Figure 3(a). The white Gaussian noises with the standard deviation 10 are scattered on the original signal to generate the noised signal as shown in Figure 3(b). The hard threshold method is used to cut off the detail coefficients up to the fifth resolution level. In every resolution level, the fixed amount of the threshold is employed for cutting off the detail coefficients. Note that since our framelets are not normalized, the amount of the threshold needs to be multiplied by the norms of the framelet filters. The

denoised signal is reconstructed from the resulting coefficients. Figure 4 shows the denoised signals for threshold 25 by different wavelet systems. One can recognize that the denoised signal by F_5 is smoother than the others. For each threshold, the averaged root mean square error (RMSE) of 20 trials between the original and the denoised signals are presented in Figure 5. As Figure 5 shows, F_5 presents the best performance among the three competitors. The reason is because our framelet systems have intermediate frequency band, which yield ternary frequency scales. Our framelet systems have more chances to cut off the detail coefficients containing the noises than Daubechies's wavelet systems without intermediate frequency band. On the other hand, from the denoised signals in Figure 4, one can recognize Gibbs phenomena, which occurs at the location of the discontinuities due to the lack of the shift invariance of the wavelet systems. The denoised signal by F_5 also presents Gibbs phenomena. However, the magnitudes of them are remarkably smaller than those of D_3 and D(7,9), which is resulted from the less shift variance of our framelet systems.

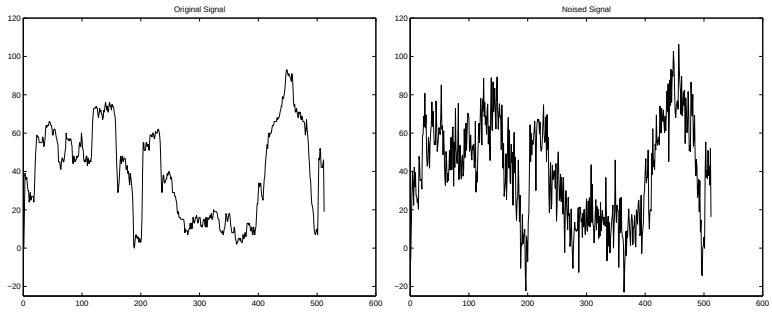

(a) Original signal (b) Noised signal

Fig. 3. The original and the noised signals with white Gaussian noises of the standard deviation 10.

4.2. *Image denoising*

In the image denoising, all the methods are the same as those of the signal denoising except that the soft threshold method and the white Gaussian noise with the standard deviation 20 are employed. Figure 6 shows the original image of Lenna of size 512 by 512 pixels and the noised one. The graph of the peak signal to noise ratio (PSNR) vs threshold of the denoised images are shown in Figure 7. The graph says that the denoised image with threshold 20 using F_5 has the highest PSNR among the others. More precisely, The highest PSNR's from the D_3, D(7,9), and F_5 are 28.677, 28.608, and 28.995 dB respectively. Figure 8 shows the denoised images with the highest PSNR's from each wavelet systems. The denoised images look very similar to each other. However, the close lookup images in Figure 9 shows the

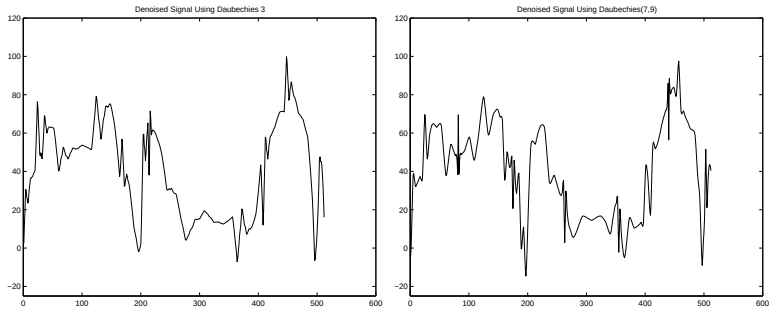

(a) Denoised signal by D_3 (b) Denoised signal by D(7,9)

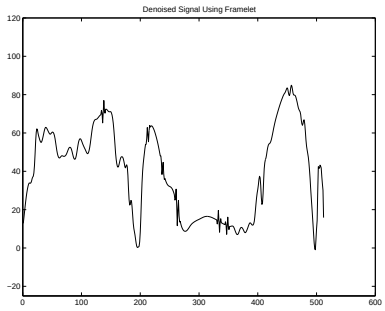

(c) Denoised signal by F_5

Fig. 4. The denoised signals using D_3, D(7,9), and F_5, from top to bottom respectively .

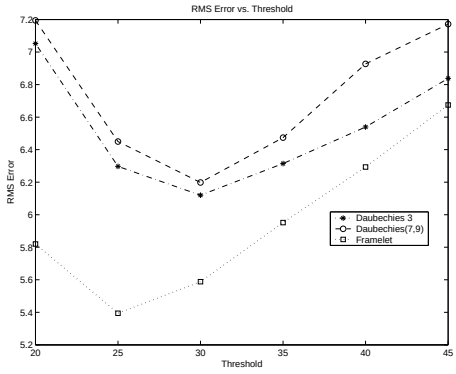

Fig. 5. The root mean square error vs threshold of D_3, D(7,9), and F_5.

differences among three images. The denoised images by D_3 and D(7,9) have Gibbs phenomena at the edges of Lenna's hat, while the denoised image by F_5 does not. This explains that F_5 has smaller shift variance than D_3 and D(7,9). On the other hand, although the denoised images in Figure 8 have the highest PSNR's, they still

present a few noises so that one might want to see the more denoised images. It is noticed that the larger threshold can make the denoised image blurred. Thus, we must choose the adequate threshold to prevent the denoised image from the blurring effect. Figure 10 shows the denoised images with the thresholds 50, 50, and 35 by D_3, D(7,9), and F_5, respectively. Again Figure 11 shows the close lookups of Figure 10. One can recognize that the images in Figure 11 are almost noiseless. However, the denoised images by D_3 and D(7,9) still have Gibbs phenomena at the edges of Lenna's hat. As a result, F_5 can denoise the image more efficiently than D_3 and D(7,9) without Gibbs phenomena due to reduced shift variance and redundant frequency scales of our wavelet frames.

(a) Original image (b) Noised image

Fig. 6. The original and the noised images with white Gaussian noises of the standard deviation 20.

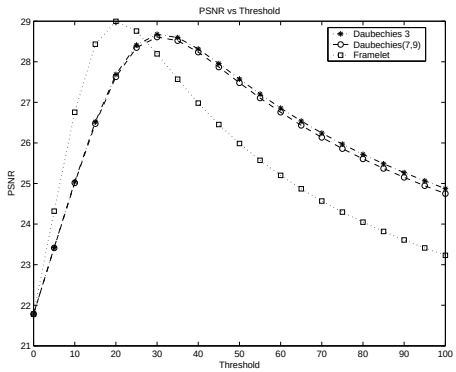

Fig. 7. The PSNR's of the denoised images by D_3, D(7,9), and F_5, respectively.

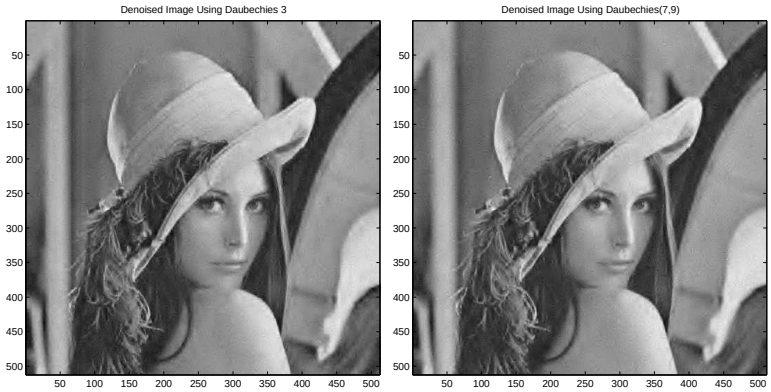

(a) Denoised image by D_3 (b) Denoised image by D(7,9)

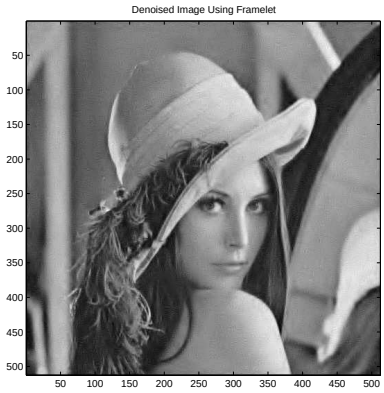

(c) Denoised image by F_5

Fig. 8. The denoised images of the highest PSNR's with the threshold 30, 30, and 20 by D_3, D(7,9), and F_5 , respectively.

4.3. *Erasure recovery*

In this section, the erasure recovery of an image is provided. Note that the orthonomal and biorthogonal wavelet systems cannot recover the erasures since the representations of functions via these systems are unique, i.e., not redundant. Therefore, the erasure recovery is allowed only to redundant framelet systems. In other words, for a framelet system to have the erasure recovery property, the redundant frequency spectrum as the ternary frequency scale of our framelet systems is needed. In the same manner as the denoising, F_5 is tested. The original image is Boat of size 512 by 512 pixels as shown in Figure 12(a). To put some erasures in the image, the original image is decomposed up to the fourth level and the randomly chosen 40% of all the wavelet coefficients is set to be zeros meaning that they are erased.

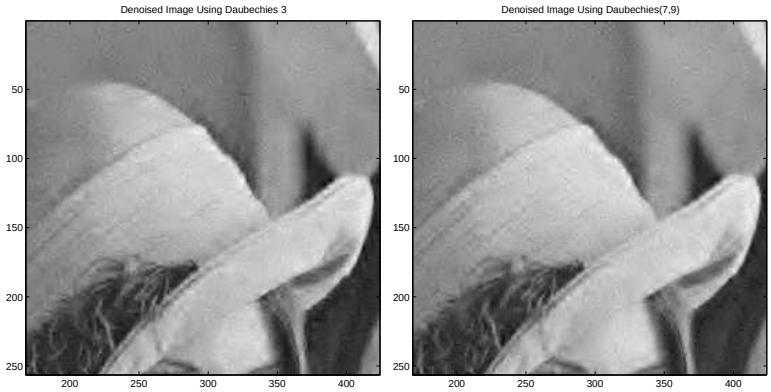

(a) Denoised image by D_3 (b) Denoised image by D(7,9)

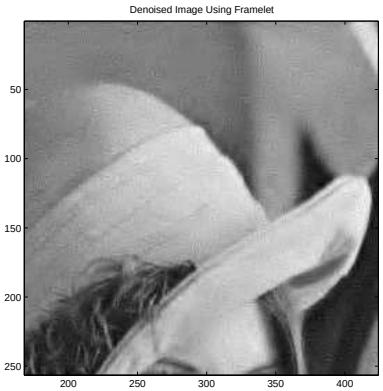

(c) Denoised image by F_5

Fig. 9. The close lookups of the denoised images of the highest PSNR's with the threshold 30, 30, and 20 by D_3, D(7,9), and F_5 , respectively.

Here, we assume that we know positions of the erased coefficients. Then, they are reconstructed to an image as presented in Figure 12(b). The PSNR of the erased image is 9.730dB. The recovery starts with the erased image. Firstly, decompose the erased image up to the fourth level. Next, wavelet coefficients of the original image excluding ones in the erased positions are copied to the corresponding positions of the present coefficients. After that, they are reconstructed to an image. These three steps are repeated certain times to obtain the recovered image. The result is shown in Figure 12(c). The PSNR of the recovered image is 39.991 dB. As one can see, the recovered image looks very similar to the original one and contain all the critical features like stays and anchors of the boats. Due to the redundant nature of our framelet systems, the erasures of the wavelet coefficients are recovered better than expected in spite of the loss of the 40% of them.

(a) Denoised image by D_3 (b) Denoised image by D(7,9)

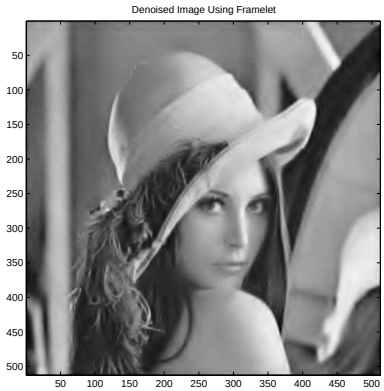

(c) Denoised image by F_5

Fig. 10. The denoised images with the threshold 50, 50, and 35 by D_3, D(7,9), and F_5 , respectively.

5. Conclusion

Tight wavelet frames with two compactly supported symmetric generators are preferable wavelet systems in theory and application since they have minimal number of redundant generators with necessary properties. To construct these wavelet frames based on MRA with high approximation orders, refinable functions with high approximation orders are needed. For this, B-splines and interpolatory refinable functions are good candidates. However, since B-splines guarantee at least one mother framelet with one vanishing moment in the UEP construction, and there are no other interpolatory refinable functions of compact support guaranteeing two symmetric mother framelets except for the piecewise linear B-spline, some extended methods are required. Several studies have employed rather difficult approaches to do this.[1 5] In Ref. 1, the authors sacrificed the compact support of the wavelets. In the present paper, sacrificing the length of support of the wavelets slightly, we

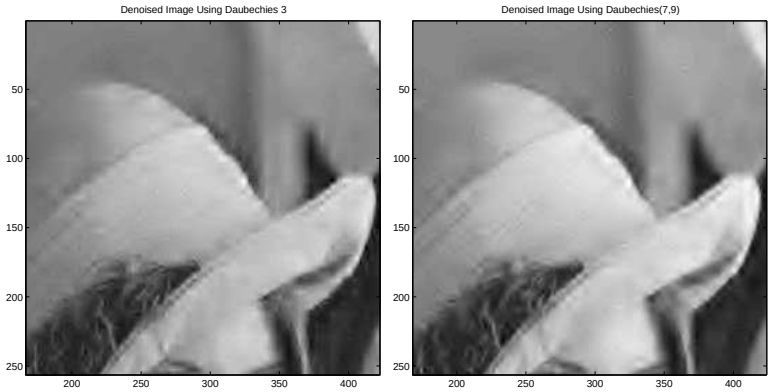

(a) Denoised image by D_3 (b) Denoised image by D(7,9)

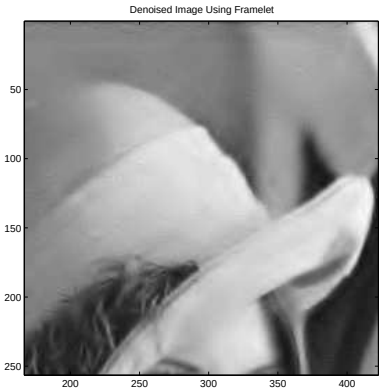

(c) Denoised image by F_5

Fig. 11. The close lookup of the denoised images with the threshold 50, 50, and 35 by D_3, D(7,9), and F_5 , respectively.

constructed the tight wavelet frame based on MRA with the same approximation orders as an interpolatory MRA. We used the quasi-interplatory subdivision masks presented in Ref. 3 as low pass filters of our framelet systems. We determined all possible free tension parameters of the quasi-interpolatory subdivision masks to construct our framelet systems. Due to computational complexity, we restricted the degree of the subdivision masks to five. For less shift variance of the wavelet transform, we employed the three times oversampling filter bank proposed in Ref. 15 and consequently made our wavelet filters have ternary frequency scales. After constructing the wavelet frames, applications to signal/image denoising and erasure recovery were provided. In order to measure the performance of our wavelet frame, we compared our results with those by Daubechies's orthonormal and biorthogonal wavelet systems. The performance of our wavelet frame was better than that yielded

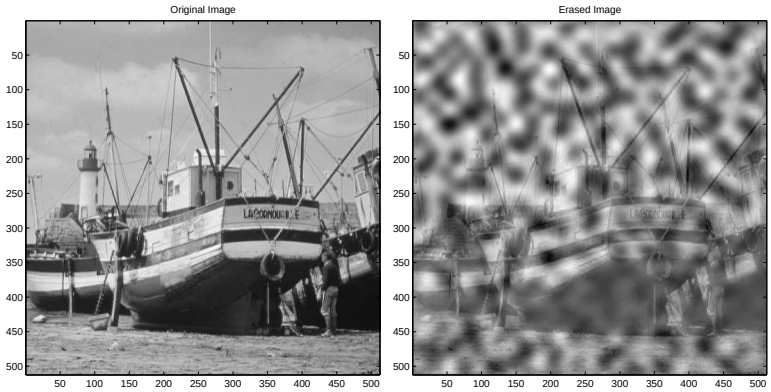

(a) Original image (b) Erased image

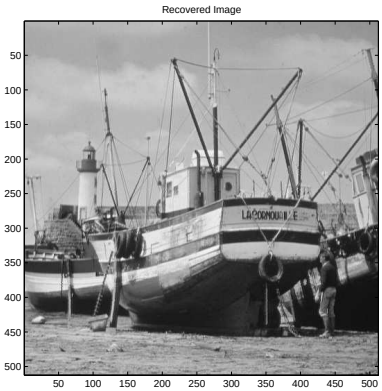

(c) Recovered image

Fig. 12. The original, erased, and recovered images from the erasures of 40% by F_5.

by Daubechies's wavelet systems for all applications presented in this paper due to reduced shift variance and redundant ternary frequency scale of our wavelet frame.

References

1. A. Z. Averbuch, V. A. Zheludev, and T. Cohen, Interpolatory Frames in Signal Space, *IEEE Trans. on Signal Processing* **54**(6) (June 2006) 2126-2139.
2. M. Choi, R.Y. Kim, M.R. Nam, H.O. Kim, Fusion of Multispectral and Panchromatic Satellite Images Using the Curvelet Transform, *IEEE Geoscience and Remote Sensing Letters* **2**(2) (2005) 136-140.
3. S. W. Choi, B.-G. Lee, Y. J. Lee, and J. H. Yoon, Stationary subdivision schemes reproducing polynomials, *Computer Aided Geometric Design* **23** (2006) 351-360.
4. C. K. Chui and W. He, Compactly supported tight frames associated with refinable functions, *Appl. Comput. Harm. Anal.* **8** (2000) 293-319.
5. C. K. Chui, W. He, and J. Stöckler, Compactly supported tight and sibling frames with maximum vanishing moments, *Appl. Comput. Harm. Anal.* **13** (2002) 224-262.

6. R. R. Coifman and D. L. Donoho, Translation-invariant de-noising, In A. Antoniadis, editor, "Wavelets and Statistics,", (Springer-Verlag Lecture Notes 1995).
7. I. Daubechies, "*Ten Lectures on Wavelets*," CBMS-NSF series in Applied Mathematics (SIAM 1992).
8. I. Daubechies, B. Han, A. Ron, and Z. Shen, Framelets: MRA-based constructions of wavelet frames, *Appl. Comput. Harmon. Anal.* **14** (2003) 1-46.
9. N. Dyn, Subdivision schemes in computer-aided geometric design, In: Light,W.A. (Ed.), *Advances in Numerical Analysis*, vol. II:Wavelets, Subdivision Algorithms and Radial Basis Functions. (Oxford University Press 1992) 36-104.
10. F. Keinert, "*Wavelets and Multiwavelets*," Studies in Advanced Mathmatics (Chapman&Hall/CRC 2004).
11. H. O. Kim, R. Y. Kim, Y. J Lee, and J. H. Yoon, Quasi-interpolatory refinable functions and construction of biorthogonal wavelet systems, preprint (2006).
12. C. A. Micchelli, Interpolatory Subdivision Schemes and Wavelets, *Journal of Approximation Theory* **86** (1996) 41-71.
13. A. Petukhov, Symmetric Framelets, *Constr. Approx.* **19** (2003) 309-328.
14. A. Ron and Z. Shen, Affine systems in $L_2(\mathbb{R}^d)$: the analysis of the analysis operator, *J. Funct. Anal.* **148** (1997) 408-447.
15. I. W. Selesnick, A higher-density discrete wavelet transform, *IEEE Trans. on Signal Processing* **54**(8) (August 2006) 3039-3048.

Table 3. Filters in the case of the degree from 1 to 5.

Degree	ω	h_0	h_1	h_2	Factor
1	$[0,1)$	ω	$-\omega$	$\sqrt{\omega(1-\omega)}$	$\frac{1}{\sqrt{2}}$
		$1-\omega$	$1-\omega$	0	
		$1-\omega$	$-1+\omega$	$\sqrt{\omega(1-\omega)}$	
		ω	ω	0	
2	$\frac{1-\sqrt{2}}{4}$	$\sqrt{2}-2$	0	$2-\sqrt{2}$	$\frac{1}{8}$
		$2\sqrt{2}$	$\sqrt{2}-2$	0	
		$2\sqrt{2}+4$	$-2\sqrt{2}$	0	
		$2\sqrt{2}$	$2\sqrt{2}+4$	0	
		$\sqrt{2}-2$	$-2\sqrt{2}$	$-2+\sqrt{2}$	
		0	$\sqrt{2}-2$	0	
	$\frac{1+\sqrt{2}}{4}$	$\sqrt{2}+2$	0	$2+\sqrt{2}$	$\frac{1}{8}$
		$2\sqrt{2}$	$\sqrt{2}+2$	0	
		$2\sqrt{2}-4$	$-2\sqrt{2}$	0	
		$2\sqrt{2}$	$2\sqrt{2}-4$	0	
		$\sqrt{2}+2$	$-2\sqrt{2}$	$-2-\sqrt{2}$	
		0	$\sqrt{2}+2$	0	
3	$-\frac{1}{64}$	1	-1	$\sqrt{14}$	$\frac{\sqrt{2}}{128}$
		-7	-7	0	
		7	-7	$-\sqrt{14}$	
		63	63	0	
		63	-63	$-\sqrt{14}$	
		7	7	0	
		-7	7	$\sqrt{14}$	
		1	1	0	
	$\frac{15}{64}$	-15	15	$3\sqrt{30}$	$\frac{\sqrt{2}}{128}$
		9	9	0	
		55	-55	$-3\sqrt{30}$	
		15	15	0	
		15	-15	$-3\sqrt{30}$	
		55	55	0	
		9	-9	$3\sqrt{30}$	
		-15	-15	0	
4	n/a				

Table 4. (*Continued*) Filters in the case of the degree from 1 to 5.

Degree	ω	h_0	h_1	h_2	Factor
5	$\frac{25(13+5\sqrt{37})}{65536}$	0.01171043446466	−0.01171043446466	0.00295927283385	
		0.00037390994039	0.00037390994039	0	
		−0.07408918655834	0.07408918655834	−0.12196386541717	
		−0.02845510739303	−0.02845510739303	0	
		0.26211647750710	−0.26211647750710	0.35109523208227	
		0.53545025322578	0.53545025322578	0	
		0.53545025322578	−0.53545025322578	−0.35109523208227	
		0.26211647750710	0.26211647750710	0	
		−0.02845510739303	0.02845510739303	0.12196386541717	
		−0.07408918655834	−0.07408918655834	0	
		0.00037390994039	−0.00037390994039	−0.00295927283385	
		0.01171043446466	0.01171043446466	0	
	$\frac{21}{32768}$	0.00045316291519	−0.00045316291519	0.00324678921738	
		0.01163118148985	0.01163118148985	0	
		−0.01780282881100	0.01780282881100	−0.07560380606177	
		−0.08474146514037	−0.08474146514037	0	
		0.14954376201241	−0.14954376201241	0.21057747209842	
		0.64802296872046	0.64802296872046	0	
		0.64802296872046	−0.64802296872046	−0.21057747209842	
		0.14954376201241	0.14954376201241	0	
		−0.08474146514037	0.08474146514037	0.07560380606177	
		−0.01780282881100	−0.01780282881100	0	
		0.01163118148985	−0.01163118148985	−0.00324678921738	
		0.00045316291519	0.00045316291519	0	

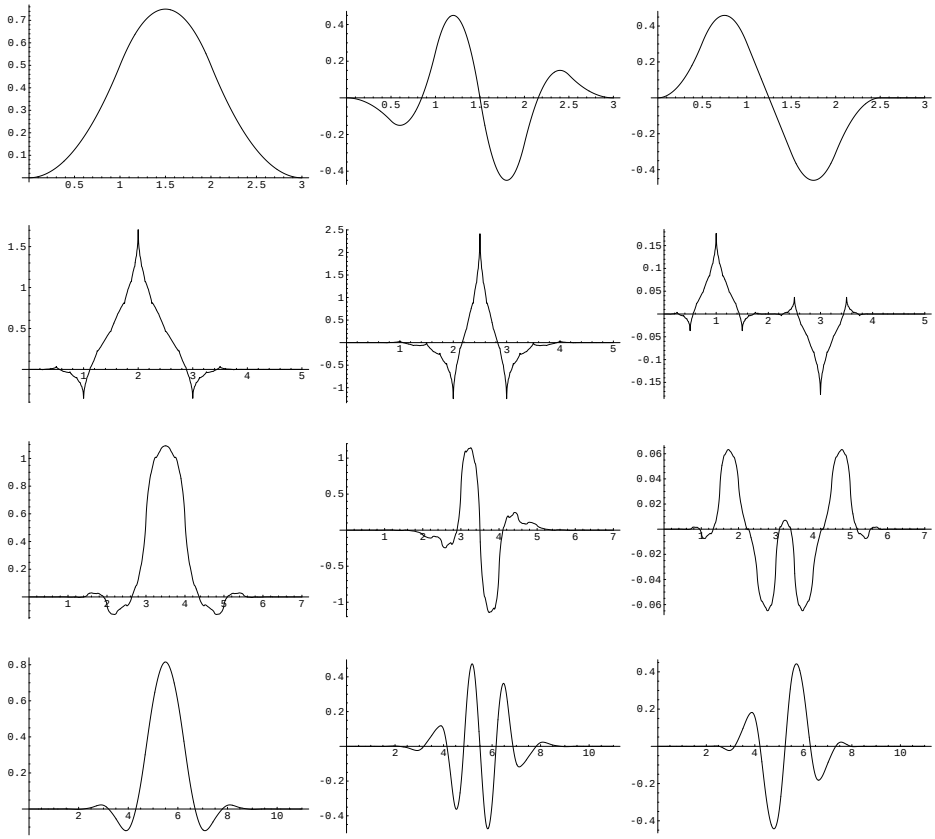

Fig. 13. Some of the refinable function ϕ's and the mother framelets ψ_1's and ψ_2's. In each row, left : ϕ, middle : ψ_1, right : ψ_2. The first row : degree 1 with $\omega = \frac{1}{4}$, the second row : degree 2 with $\omega = \frac{1-\sqrt{2}}{4}$, the third row : degree 3 with $\omega = -\frac{1}{64}$, and the fourth row : degree 5 with $\omega = \frac{25(13+5\sqrt{37})}{65536}$.

Table 5. The Hölder continuity of the refinable functions with various tension parameters in the degree L = 1, 2, 3, 4, and 5. The parameters which provide the maximum smoothness in each degree are included.

Degree	Tension parameter ω	Hölder continuity
1	$\frac{1}{16}$	0.19264507794240
	$\frac{1}{8}$	0.41503749927884
	$\frac{1}{4}$	2^*
	$\frac{1}{2}$	1
	$\frac{3}{4}$	0.41503749927884
	$\frac{7}{8}$	0.19264507794240
2	$\frac{1-\sqrt{2}}{4}$	0.5
	$\frac{1}{8}$	3^*
	$\frac{1+\sqrt{2}}{4}$	0.5
3	$-\frac{1}{64}$	2.67807190511264
	$\frac{5}{128}$	2.83007499855769*
	$\frac{15}{64}$	0.24511249783653
4	$\frac{3}{128}$	3.67807190511264
5	$\frac{21}{32768}$	2.16993910723648
	$\frac{63}{8192}$	4.49220535980130*
	$\frac{25(13+5\sqrt{37})}{65536}$	3.09395033834313

* : the maximum smoothness in each degree.

Table 6. The approximation order of the refinable functions and the vanishing moments of our framelets with various parameters in the degree L = 1, 2, 3, and 5.

Degree	Tension parameter ω	Approximation order of	Vanishing moments of		
		ϕ	ψ_1	ψ_2	ψ_3
1	$\frac{1}{16}$	1	1	1	1
	$\frac{1}{8}$	1	1	1	1
	$\frac{1}{4}$	3	3	1	1
	$\frac{1}{2}$	1	1	1	1
	$\frac{3}{4}$	1	1	1	1
	$\frac{7}{8}$	1	1	1	1
2	$\frac{1-\sqrt{2}}{4}$	2	2	1	1
	$\frac{1+\sqrt{2}}{4}$	2	2	1	1
3	$-\frac{1}{64}$	3	3	2	2
	$\frac{15}{64}$	3	3	2	2
5	$\frac{21}{32768}$	5	5	3	3
	$\frac{25(13+5\sqrt{37})}{65536}$	5	5	3	3